Full-length article

2D and 3D PVA electrospun scaffold evaluation for ligament implant replacement: a mechanical testing, modelling and experimental biomechanics approach

Elisa Roldán [1,*], Neil D. Reeves [2], Glen Cooper [3], Kirstie Andrews [1]

1 Department of Engineering, Faculty of Science & Engineering, Manchester Metropolitan University, Manchester M1 5GD, UK. Elisa.Roldan-Ciudad@mmu.ac.uk.
2 Department of Life Sciences, Faculty of Science & Engineering, Manchester Metropolitan University, Manchester M1 5GD, UK
3 School of Engineering, University of Manchester, Manchester M13 9PL, UK
* Correspondence: Elisa.Roldan-Ciudad@mmu.ac.uk.

Abstract:

The gold standard to characterise anterior cruciate ligament (ACL) implants is through the evaluation of mechanical properties such as Young's modulus or ultimate tensile stress. Currently, no studies have been performed to relate the *in-vivo* hyper-elastic behaviour of the ACL with the design of tissue engineered ligaments. The aim of this work is to determine the most comparable 2D/3D polyvinyl alcohol (PVA) electrospun structure to the *in-vivo* mechanical behaviour of the natural ligament. Biomechanics of 12 young participants were captured while daily and high impact activities were performed. A musculoskeletal knee model and kinematic data were used to estimate the *in-vivo* ACL length and strain. The *in-vivo* ACL tensile forces were determined with a non-linear force/strain relationship. 2D scaffolds, 1 twisted filament scaffolds, 3 twisted filaments scaffolds and 3 twisted/braided filaments scaffolds were fabricated using electrospinning and characterised morphologically and mechanically using scanning electron microscopy and tensile testing respectively. Cyclic tensile and shear tests were performed in dry and wet conditions to crosslinked and non-crosslinked samples. The hyper-elastic behaviour of our PVA scaffolds was characterised with the Mooney Rivlin model and a non-linear string-based model, and both models compared with the *in-vivo* mechanical behaviour of the native ACL. Crosslinked 3 twisted/braided filaments scaffolds faithfully mimicked the morphology and the hyper-elastic behaviour of the natural ACL, showed a good resistance to shear loading and remained undegraded in phosphate-buffer saline solution. This study demonstrated, for the first time, that 3 twisted/braided filaments PVA electrospun scaffolds have an excellent potential for ACL replacements.

Keywords: Anterior cruciate ligament (ACL), biomimetic 3D electrospun scaffolds, motion capture, knee model, hyper-elastic behaviour.

1. Introduction

The ACL rupture is the most common injury in the knee joint [1]. Due to its low vascularization, this ligament has very poor healing mechanisms, making the use of ACL grafts necessary for its reconstruction or replacement [1]. Currently, the gold standards for ACL replacement are the patella-tendon, hamstring-tendon and quadriceps-tendon autografts [1]. However, the autografts exhibit various disadvantages, such as donor site morbidity, long rehabilitation time or lack of availability, potentially solved through the implantation of tissue engineered grafts [2].

An ideal tissue engineered ACL should be biocompatible (able to perform with an appropriate host response in a specific application); have an appropriate degradation rate in accordance to the tissue formation; should exhibit mechanical behaviour comparable to the natural ligament [1,2]; and ideally, should mimic the hierarchical structure of the ligament and its extracellular matrix in order to promote cell proliferation and imitate mechanical response. In terms of mechanical behaviour, ACL replacements should be able to replicate not only the linear region, presenting maximum tensile stress of approximately 38 MPa [3] and a Young's modulus of about 111 MPa [3], but the non-linear behaviour of the *in-vivo* natural ACL, exhibiting comparable models for the toe, linear and breaking regions. Moreover, the ACL has demonstrated to exhibit a hyper-elastic behaviour with a complex non-linear relationship between the stress and strain [4,5]; however, this behaviour was never assessed for ACL replacements to date, and there is a need of comparing

the hyper-elastic behaviour of the *in-vivo* natural ligament with the one of the manufacture substitutes. Regarding the morphology of the scaffolds, the fibres should be between 40 and 150 nm in diameter mimicking the collagen fibrils in the ACL, the bundle of fibres approx. 1 to 20 μm, and the filaments between 360 and 1500 μm in diameter simulating the fascicles of the natural ACL [6–10]. Moreover, a bimodal distribution of the diameters was observed in healthy ACLs and non-observed in injured ACLs [11]. In healthy ACLs, two peaks were observed in diameters of 95±10 nm and in diameters of 160 nm [12].

PVA is a promising polymer for tissue engineering applications due to its biodegradability, non-toxicity, biocompatibility [10,13,14] and appropriate mechanical properties [15,16]. Its water solubility and nontoxicity make PVA a great alternative specially for electrospun manufacture, since it is water soluble prior to cross-linking negating the need for extraction of toxic vapours from solvents that are required by other polymers. However, PVA is a biodegradable polymer; therefore, in order to decrease its degradation rate allowing for cell infiltration, the scaffolds should be exposed to a crosslinking agent. The effect of the crosslinking technique on the morphology and mechanical properties of 2D and 3D electrospun scaffolds were studied in this article.

Nowadays, there are different techniques that try to create tissue engineered implants, in particular ligaments and tendons, with a 3D structure: twisting, braiding, weaving, knitting and combinations of the above-mentioned [17]. It is known that by modifying the geometrical pattern of the structure its mechanical properties can be changed [17,18]. Braided structures are designed to transfer large loads, bearing axial and shear loads and provide torsion stability [17,19]. Twisted fibres are used to improve the abrasion resistance and flexibility [17,18]. Fibres of silk [20,21], poly L-lactic acid [17,22], polylactide-co-glycolic acid [22,23] and polyglycolic acid [22] were purchased and then twisted [17,20,21,24], braided [17,22,23] and a combination of both [17] forming bundles of fibres simulating the ligamentous or tendinous structures; however, the nanostructure of the extracellular matrix (ECM) was not achieved with this technique and the mechanical properties of these scaffolds did not fully mimic the mechanical behaviour of the ACL.

The electrospinning technique allows the creation of a network of nanofibres similar to the ECM of soft tissue [25]. Currently, some studies were found using 3D electrospun scaffolds with the aim of manufacturing tendons [26–28] and ligaments [12,29,30]. However, so far, there is not any study focussed on developing 3D electrospun scaffolds with the purpose of replicating the *in-vivo* hyper-elastic behaviour of the native ACL.

Bosworth *et al*., investigated the mechanical behaviour between 2D PCL electrospun scaffolds with randomly and aligned distributed fibres and 3D PCL twisted electrospun scaffolds with the purpose of producing tissue engineering tendons [26]. The conclusions of that study were that 3D electrospun bundles exhibited ten times more ultimate tensile stress than 2D electrospun scaffolds with randomly distributed fibres, and 2D electrospun scaffolds with aligned fibres showed three times more ultimate tensile stress than the same scaffold but with randomly distributed fibres. However, the in-vitro results obtained were far from the mechanical properties of the native ACL (ultimate tensile stress 38 MPa and Young's modulus 111 MPa [3]), reporting a Young's modulus of 14.11 MPa and an ultimate tensile stress of 4.74 MPa [26]. Sensini *et al*., mechanically evaluated one filament twisted electrospun scaffolds manufactured with PLLA/Coll-75/25, PLLA/Coll-50/50 and pure PLLA, concluding that dry PLLA/Coll-75/25 samples exhibited the highest ultimate tensile stress of 15 MPa [27], inferior to the natural ACL that exhibits an ultimate tensile stress of 38 MPa. Mounthy *et al*., developed a 3D electrospun structure by manually twisting four filaments of polydioxanone (PDO) together, obtaining ultimate tensile stress between 45 and 48 MPa [29], superior to the natural ACL (38 MPa); however, Young's modulus between 60 and 80 MPa, inferior to the 111 MPa exhibited by the natural ACL, corresponding to laxity problems of the structure. Rothrauff *et al*., studied the mechanical properties of PCL and PLLA braided and stacked electrospun scaffolds [30]. In that study, the highest ultimate tensile stress was 20 MPa, found in PCL braided electrospun scaffolds, inferior to the natural ACL. Young's modulus and ultimate tensile stress were calculated in all those studies to mechanically assess their scaffolds; however, these properties only characterise the linear elastic behaviour of the material, without considering the hyper-elastic behaviour of the *in-vivo* natural ACL or the mechanical behaviour of the scaffolds under physiological conditions.

The aim of this study was to assess the suitability of different 2D and 3D PVA electrospun structures to create biomimetic ACL replacements which could replicate the *in-vivo* mechanical behaviour of the native ACL. In order to achieve that goal, crosslinked and non-crosslinked 2D and 3D structures were mechanically analysed under cyclic loading, in dry and wet conditions and under tensile and shear test. A hyper-elastic Mooney Rivlin model and a non-linear string-based model describing the toe, linear and breaking regions were performed for our PVA scaffolds and compared to the hyper-elastic and non-linear models performed with the *in-vivo* mechanical behaviour of the ligament calculated from data published in Roldan *et al* [31]. In addition, the morphology of the scaffolds was studied and compared to the natural ACL.

The novel approaches used in this article to characterise the hyper-elastic behaviour of electrospun scaffolds, mimic the physiological conditions and multidirectional failure mechanisms of the native tissue and evaluate the *in-vivo* mechanical behaviour of the natural tissue can be applicable to design biomimetic replacements for a wide range of human tissues.

2. Materials and Methods

2.1. Materials

A homogeneous solution of 12% w/v of PVA (#P8136) and distilled water (dH_2O) was prepared by heating at 100°C and stirring the solution for one hour. PVA was acquired from Sigma Aldrich (UK).

25% glutaraldehyde (#G5882) purchased from Sigma Aldrich (UK) was used to fabricate the crosslinked samples.

2.2. Manufacturing process

Twelve electrospinning sheets were created with an electrospinning device (Prefector, Spraybase®, Maynooth, Ireland), a flow rate of 1 ml/h, an 18 G needle, high voltage of 20 kV and a distance between the needle and the collector of 8 cm. The manufacturing parameters were optimised following previous studies [10,25]. The fibres were projected to a 30 x 30 aluminium foil attached to a 9.65 cm diameter rotating collector working at 2000 rpm. All the electrospinning sheets were manufactured at room temperature (25°C) and for 3 hours spin time [32].

2.2.1. Fabrication of the 2D electrospun samples

Non-crosslinked 2D structure samples were created by cutting in a dog-bone shape the manufactured electrospun sheets. The same manufacture procedure was used to generate the crosslinked 2D samples, which were exposed to a crosslinker agent for 24 hours. A total of 40 2D electrospun samples were produced.

2.2.2. Fabrication of the 3D electrospun samples

Three different types of 3D electrospun structures were created: 1 filament scaffolds, 3 twisted filaments scaffolds and 3 twisted/braided filaments scaffolds. To manufacture these scaffolds, the electrospun sheets were cut into rectangles of 2 x 15 cm, carefully pealed from the aluminium foil, manually twisted clockwise to form a long-packed filament and cut each filament in half. 1 twisted filament scaffolds were the result of the procedure described above. 3 twisted filaments scaffolds were fabricated by twisting together three of the 1 filament scaffolds, the three filaments were twisted together, in a clockwise manner, until a packed and stable structure was created following a previous study [16]. 3 twisted/braided filaments scaffolds were manufactured by manually braiding three twisted filaments with angles of 35±2°. 40 samples of each 3D electrospun structures were created.

Crosslinked and non-crosslinked 3D electrospun samples were manufactured in the same manner.

2.3. Crosslinking process

25 ml of 25% glutaraldehyde (GTA) was poured into a Petri dish at the bottom of the desiccator, then the samples to be crosslinked were placed on a cardboard frame over a metallic mesh on top of the Petri dish and the desiccator was sealed. The samples were exposed to GTA vapour for 24 hours inside the desiccator. After the crosslinking process, the samples were dried under a fume hood for 24 hours in order to remove the moisture and minimise the toxicity of the samples. The crosslinking process was performed following previous studies [32].

2.4. Mechanical characterisation

Three different mechanical assays were performed to evaluate the mechanical behaviour of the non-crosslinked and crosslinked 2D and 3D structures: Cyclic tensile tests with dry samples, cyclic tensile test with wet samples and cyclic shear tests with dry samples. A total of 168 samples were mechanically tested, 10 crosslinked and non-crosslinked samples per structure (2D, 1 filament scaffolds, 3 twisted filaments scaffolds and 3 twisted/braided filaments scaffolds) and testing condition (dry/wet and tensile/shear).

The 2D samples were prepared by cutting the scaffold mesh with a dog-bone cutting die (25 x 4 mm, test length x width). The 3D samples were manufactured as described in section 2.2.2. All samples were separately attached on cardboard frames to maintain the sample alignment in the tensometer (Instron H10KS, US). Both sides of the cardboard were cut after the alignment and before testing.

The thickness of each sample was measured three times with a digital calliper, an analogue calliper and through SEM images in order to accurately determine the nominal cross-sectional area of each scaffold, calculated from the mean of all the measurements taken.

Each sample was subjected to ten loading cycles and then tested to failure. The ACL exhibits a maximum % strain of 13% in a gait cycle [31,33]; therefore, each loading cycle stretched the sample up to 13% strain, mimicking 10 gait cycles to precondition the samples [34]. In terms of Young's modulus, no significant differences were observed for gait cycles between 10 and 20 [35]; therefore the number of gait cycles was optimised to 10 cycles. All the mechanical tests were performed at room temperature (25°C) with identical set up of the tensometer: 100 N load cell, 5 mm/min test speed and rubber pneumatic clamps were used to reduce stress concentrations [36].

The ACL is an extra-synovial intraarticular ligament [37]. It is not immersed in synovial liquid; however, it is placed in a wet environment. To mimic the environmental conditions, 10 crosslinked samples per 2D and 3D structure were immersed in phosphate-buffer saline solution (PBS) for 1 minute before being tested. The immersion time was optimised considering intervals of time from 1 minute to 60 minutes and calculating the mechanical properties per interval of time. In terms of Young's modulus and ultimate tensile stress, no significant differences were observed for samples immersed for 1 minute and 60 minutes [35]. Testing in wet conditions was performed within the next minute after removal from PBS to keep the moisture and under the same set up indicated above; however, due to the elastic character of the PVA in wet conditions a preload of 0.1N was added to fully align the sample in the tensometer.

The anterior/posterior shear force experienced by the ACL was mimicked with the tensometer (Figure 1), placing the samples with the same angle of inclination of the native ACL in the sagittal plane (approximately 50° [38–40]) in a cardboard frame. The angle was obtained from the MRI of the right knee from our participants and corroborated from the literature [38–40]. As with the other samples, both sides of the cardboard were cut before being tested under the set up described above.

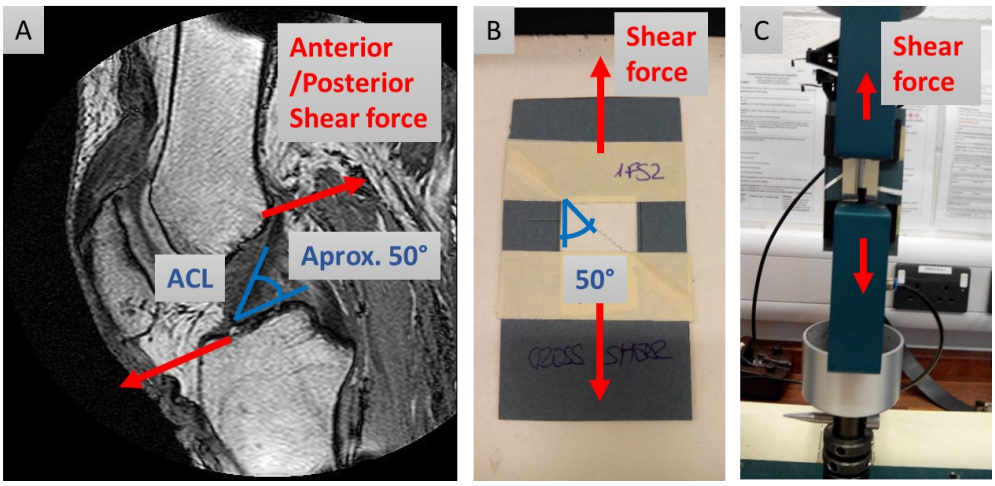

Figure 1. A) MRI of the right knee showing the anterior/posterior shear force and ACL angle in the sagittal plane, B) Angle of inclination of the samples and simulated anterior/posterior shear force experienced by 1 twisted crosslinked filament scaffold, and C) Applied force in a tensometer.

Stress / Strain (%) curves and mechanical properties including Young's modulus calculated for the last loading cycle and in points in between the transition and deflection stage (between 11% and 12% strain in most of the dry scaffolds), shear modulus, ultimate tensile stress and strain at break were analysed for each crosslinked and non-crosslinked sample under dry and wet conditions. The calculation of these properties will help us to initially assess which structure could replicate the mechanical behaviour of the native ACL.

Once the most suitable structure was determined, a hyper-elastic Mooney Rivlin model and a novel non-linear spring model based on Blankevoort and Huiskes model [41] were applied to experimental data from the scaffolds and *in-vivo* mechanical behaviour of the ACL. Experimental data from the most appropriate structure was found from the average of the tensile stress/strain data of the ten samples produced for that specific structure, surface treatment (crosslinked/non-crosslinked) and testing condition (dry/wet). Equation 1 expresses the Mooney Rivlin equation for the uniaxial tensile test, where C_1 and C_2 are the coefficients of the model in MPa and λ is the stretch defined as equation 2 [42].

$$\sigma = 2C_1\left(\lambda^2 - {}^1/_{\lambda}\right) - 2C_2\left(\lambda^2 - {}^1/_{\lambda}\right) \qquad (1)$$

$$\lambda = \varepsilon + 1 \qquad (2)$$

Equations 3, 4 and 5 represent the equations used in the non-linear springs model based on Blankevoort and Huiskes model [41]. Where equation 3 represents the toe region, equation 4 the linear region and equation 5 the breaking region. It is worth notice that equation 5 was only determined for modelling the mechanical behaviour of our scaffolds, since breaking region was not observed in our *in-vivo* mechanical behaviour.

$$\sigma = A\varepsilon^2 \qquad 0 \le \varepsilon \le \varepsilon_t \qquad (3)$$

$$\sigma = k_1(\varepsilon - B) \quad \varepsilon_t \le \varepsilon \le \varepsilon_i \qquad (4)$$

$$\sigma = C + k_2\varepsilon \qquad \varepsilon_i \le \varepsilon \qquad (5)$$

Where ε_t and ε_i are the strain at the transition and inflection point respectively (adimensional), A (in MPa), B (strain in %) and C (adimensional) are constants of the model and k_1 and k_2 are the slope of the curve (in MPa) in the linear and breaking regions.

To determine the constants and coefficients of the model that best fit the experimental data with the hyper-elastic and non-linear spring models, the Solver tool implemented in Excel version 2308 was used. These parameters were determined minimising the sum of squared errors. The goodness of the fit for the models was assessed by the coefficient of determination.

2.5. Morphological characterisation

Five studies have been performed to characterise the morphology of 3D structures: study of the morphology of non-crosslinked structures, influence of crosslinking agent on the morphology of the structures, consequence of wet conditions on the morphology of crosslinked samples, effect of tensile forces on the morphology of the structures and diameter distribution.

A SC7640 sputter coater (Quorum Technologies Ltd. Kent, UK) was used to coat the samples with gold prior to their visualization with a field emission scanning electron microscope, Zeiss Supra 40 (FE-SEM, Carl Zeiss SMT Ltd., Cambridge, UK). The intensity used for coating the samples was 20 mA, the voltage 0.8 kV and the duration of the coating was 120 seconds, which provided a coating thickness of 32.6 nm following equipment specifications. SEM images were taken between 5- and 6-mm working distance, at 2 kV and with magnifications of 100x, 1000x, 5000x and 20000x in order to measure the nanofibres, the bundle of fibres and fascicles. Two images for each magnification and scaffold were taken and ten scaffolds for each 2D/3D structure and each set of experiments were analysed. Fibre diameter and thickness of the bundles of fibres and fascicles were determined with AxioVision SE64 Rel. 4.9.1 software (Carl Zeiss SMT Ltd., Cambridge, UK) by measuring 20 fibres/image in two 20000x magnification SEM images, 3 bundles of fibres/image in two 5000x magnification SEM images and the fascicles of each sample in two 100x magnification SEM images, for each 3D structure and each set of testing conditions.

The dimensions of the fibres, bundles and fascicles of the scaffolds were compared with the dimensions of the fibrils, fibres and fascicles of collagen in the native ACL found in the literature [6–10]. Moreover, the diameter distribution our samples was evaluated through a histogram and a polygon of frequencies, and compared to the diameter distribution of the fibrils of collagen in healthy ACLs following a recent study [12].

2.6. In-Vivo Estimation of ACL mechanical behaviour– Gait Laboratory Measurements

2.6.1. Participants

Twelve young knee/hip healthy adults participated in this study: 7 men and 5 women; mean ± SD age: 27.3 ± 3.3 years, height: 1.7 ± 0.09 m and mass: 71.6 ± 15.5 kg. For inclusion propose, the participants completed two standardised surveys, the Knee Injury and Osteoarthritis Outcome Score (KOOS) and the Hip Injury and Osteoarthritis Outcome Score (HOOS) tests. All participants gave written and signed consent prior the experimental work was carried out.

All research and methods were performed in accordance with the Declaration of Helsinki and were approved by the ethics committee of the Manchester Metropolitan University (Approval Number: SE141530).

2.6.2. Protocol

10-camera motion capture system (Vicon 612 system, Oxford Metrics, UK) and 33 reflective markers placed on specific anatomical landmarks of each participant were used to collect the kinematics of the participants while activities including walking, running, crossover cutting, sidestep cutting, dropping from a 30 cm height jumping box and jump vertically with both legs at maximum effort, and jumping horizontally three times with one leg were performed. The activities were executed at participants' self-selected speed and for three successful repeated trials. The kinematic data was sampled at 100 Hz. A full protocol description can be found in a previous study [31].

Data processing and kinematics analysis were carried out with Vicon Nexus 1.8.5. software (Vicon Motion Systems Ltd., UK) and OpenSim 3.3 (Sim TK, Stanford, CA) respectively.

2.6.3. ACL length, strain and force estimation

The *in-vivo* right ACL length was determined at each timeframe by tracking the coordinates of the modelled insertion points of the right ACL, through a 27 degree of freedom (DOF) OpenSim model with 3 DOF for the knee, 12 bones and 92 musculotendon actuators [43]. Equations 6 and 7 were used to calculate the *in-vivo* right ACL strain at each timeframe.

$$\varepsilon = \frac{L - L_0}{L_0} \quad (6)$$

$$L_0 = \frac{L_r}{(\varepsilon_r + 1)} \quad (7)$$

Where L_0 is the zero-load length, Lr is the right ACL length at knee full extension for each subject and ε_r is the reference stain of 0.08 taken from Blankevoort and Huiskes [41].

The *in-vivo* ACL tensile forces were estimated with a well-established force/strain relationship presented in Blankevoort and Huiskes [41], in parallel with a damping element to mimic the viscoelastic behaviour of the natural ligament [43]. The *in-vivo* tensile forces exerted by the non-linear spring (F_1) were calculated following the equations 8, 9 and 10, where ε was the *in-vivo* strain of the ligament at each timeframe, ε_l was the linear range threshold (0.03 [41]) and k was the stiffness of the spring (500 N [41]).

$$F_1 = \frac{k\varepsilon^2}{4\varepsilon_l} \qquad 0 \le \varepsilon \le 2\,\varepsilon_l \quad (8)$$

$$F_1 = k(\varepsilon - \varepsilon_l) \qquad \varepsilon > 2\,\varepsilon_l \quad (9)$$

$$F_1 = 0 \qquad \varepsilon < 0 \quad (10)$$

The *in-vivo* tensile forces exerted by the damper (F_2) were estimated following the equation (11), where D was the damping coefficient (500 N s/m [44]) and v was the velocity of the ligament calculated by the central difference method.

$$F_2 = D\,v \quad (11)$$

In-vivo stresses were estimated dividing the *in-vivo* ACL tensile forces by the cross-sectional areas of the ACL of our participants measured through magnetic resonance imaging (MRI) with a T1 spin echo sequence (FS: 0.25; TR: 1050; TE: 26 and T: 3.5 mm). The measured cross-sectional areas (29±2 mm) were in accordance to a previous research [45]. A full description of ACL length, strain and force estimation, and their results can be found in Roldán *et al.* [31].

2.7. Data analysis

Mean and standard deviation (Std Dev) were calculated for each of the structural and mechanical properties for all 2D and 3D crosslinked and non-crosslinked structures.

In order to compare the mechanical properties (ultimate tensile stress and Young's modulus) between the 2D and 3D scaffolds, crosslinked and non-crosslinked samples from the same structure and testing conditions (dry/wet and tensile/shear), a Multivariate Analysis of Variance (MANOVA) with a 95% confidence was performed. In addition, the effect sizes produced for the exogenous variables and their interactions on the endogenous variables were found with the partial squared Eta values provided by the MANOVA. Small effects are represented by values lower than 0.01, values of 0.06 produce average effects, and values higher than 0.14 produce very high effects in that factor or interaction [46]. The study of partial squared Eta values allows us to understand the contribution of the crosslinking effect or wet environment on the mechanical properties.

Moreover, six one-way ANOVAs were performed to determine the optimum number of cycles for the cyclic mechanical tests, optimum immersion time for wet condition testing, significant differences in the mechanical behaviour

(ultimate tensile strength, Young's modulus and strain at break) with the cadaveric and *in-vivo* ACL and the significance of the structure, crosslinking and testing conditions on the morphology of the fibres. Differences were considered significant for p value <0.05.

All statistical analyses were conducted using SPSS (IBM Inc, US).

3. Results and Discussion

3.1. Mechanical characterisation

3.1.1. Initial mechanical assessment

Ten samples for each crosslinked and non-crosslinked structure were analysed after 10 loading cycles. The structure with the highest ultimate tensile stress was the 1 twisted filament scaffold, with 37 ± 4 MPa for the non-crosslinked samples and 54 ± 14 MPa for the crosslinked samples (Figure 2). The 3 twisted/braided filaments crosslinked samples with 38 ± 3 MPa exhibited non-significant differences with the tensile stress of the cadaveric ACL (38 MPa [3]).

As expective, 1 twisted filament scaffolds and 3 twisted/braided filaments crosslinked scaffolds, demonstrated to have enough ultimate tensile stress to bear the maximum average *in-vivo* stresses (24.8 ± 2.2 MPa) experienced for the participants while performing a maximum effort jump (Figure 2). Moreover, dry 2D and 3 twisted filaments crosslinked samples exhibited enough ultimate tensile stress to perform activities such as walking (17.6 ± 0.3MPa), sidestep and crossover cutting (16.2 ± 5.8 MPa and 14.6 ± 5.1 MPa respectively) or running (12.6 ± 3.9 MPa), as shown in Figure 2.

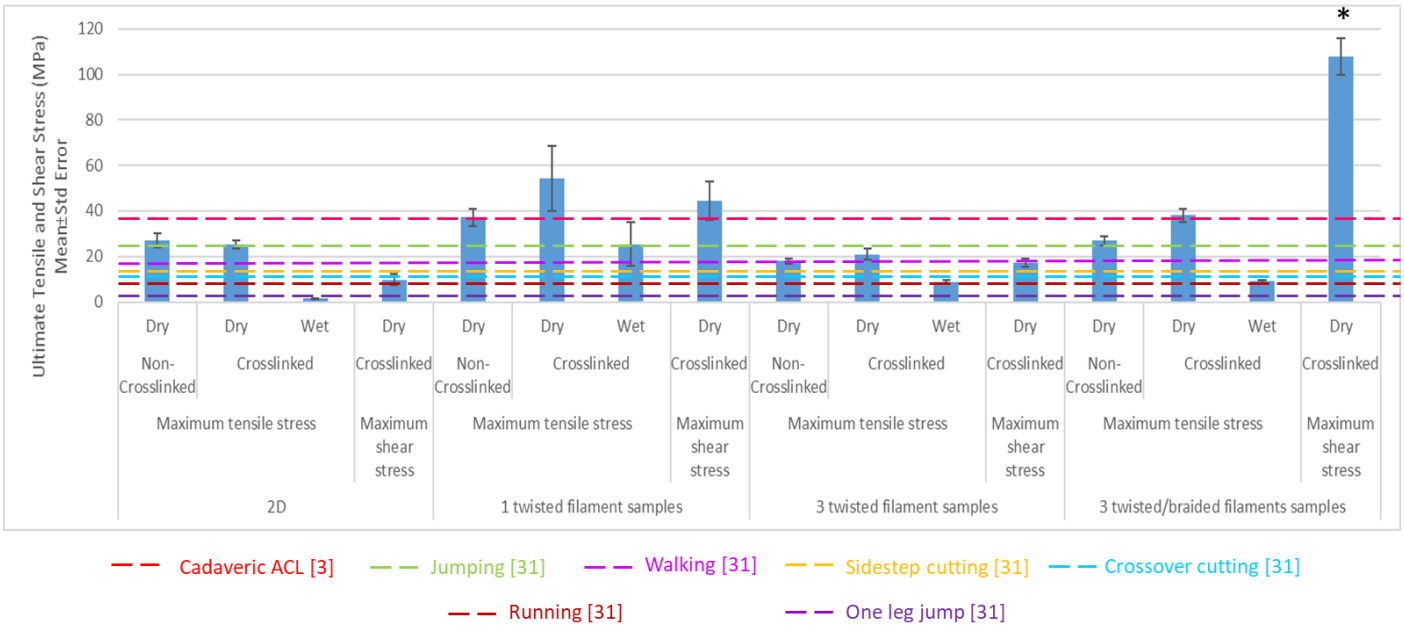

Figure 2. Ultimate tensile and shear stress (MPa) after 10 loading cycles per electrospun structure (Mean ± Std Dev). * Significant different with the cadaveric and *in-vivo* ACL (p value < 0.05).

3 twisted/braided filaments samples experienced a Young's modulus of 129 MPa for non-crosslinked samples and 149 MPa for crosslinked samples. This structure exhibited the closest values of Young's modulus to the natural ACL for non-crosslinked and crosslinked samples. Figure 3 shows the Young's modulus (Mean ± Std Dev) for all of the analysed scaffolds.

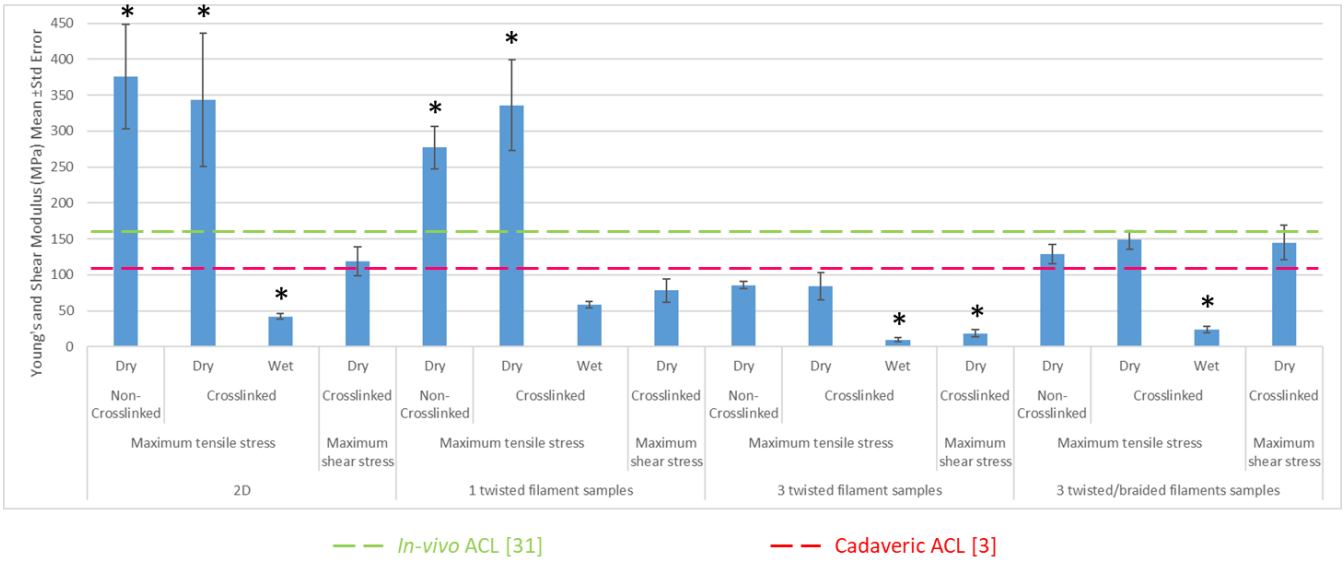

Figure 3. Young's modulus and shear modulus (MPa) after 10 loading cycles per electrospun structure (Mean ± Std Dev). * Significant different with the cadaveric and *in-vivo* ACL (p value < 0.05).

Dry 2D and 1 twisted filament scaffolds structures reached Young's modulus superior to cadaveric studies reported previously and to the Young's modulus calculated through our *in-vivo* biomechanical study (Figure 3). However, the scaffolds with non-significant differences in the mechanical behaviour to the natural ACL in wet condition were the 1 twisted filament scaffolds with ultimate tensile stress of 37.2 ± 12.1 MPa and Young's modulus of 73.9 ± 15.6 MPa.

As demonstrated in Roldan et.al [31,43] not only the tensile properties have to be considered in the design of a ACL implant. The failure mechanics of the natural ACL were due to multidirectional loading; therefore, it was also important to determine how the scaffolds behaved under shear loading, more specifically under anterior/posterior shear loading since the ligament restricts the anterior/posterior displacements. In this study, 2D and 3D scaffolds were tested under shear load, mimicking the anterior/posterior shear force experienced by the ACL during sudden stops or changes of direction, that normally occur during high impact activities such as crossover or step-side cutting. The 3 twisted/braided filaments crosslinked structure exhibited the highest maximum shear stress compared with the other structures, allowing the samples to bear higher shear loads than the rest of the structures. This fact is in agreement with previous studies [47,48], where it was demonstrated that braiding techniques can bear and transfer axial loads, improving shear resistance and providing mechanical reinforcement. The highest shear modulus was observed in 3 twisted/braided filaments crosslinked samples with a value of 144 MPa and the minimum value was experienced for the 3 twisted filaments crosslinked samples with a mean value of 18 MPa. Due to the fact that the ACL is normally mechanically characterised under axial loads, very few studies have been done to calculate the shear modulus of the natural ACL. However, one computational study found that the short-term shear modulus of the ACL was 68 MPa and the long-term shear modulus was 45 MPa [49], being all the manufactured scaffold able to reach those values with the exception of 3 twisted filament scaffolds.

In terms of strain at break, all our developed scaffolds, except for the 2D scaffolds tested in wet conditions, exhibited higher strain at break than the maximum average *in-vivo* strain calculated from the kinematics of our participants (Figure 4). Where maximum average *in-vivo* strain of 17.5 ± 1.3% was observed for a maximum effort jump, 13.2 ± 0.2% was observed during walking, 10.7 ± 4% and 10.7 ± 3% were observed for sidestep and crossover cutting respectively and 8.8 ± 0.4% and 8.9 ± 0.4% were observed for ascending and descending stairs [31,43]. And all 3D scaffolds developed in this study and tested in dry and wet conditions exhibited higher strain at break than the strain at break reported from cadaveric ACLs (44 ± 8%) [3].

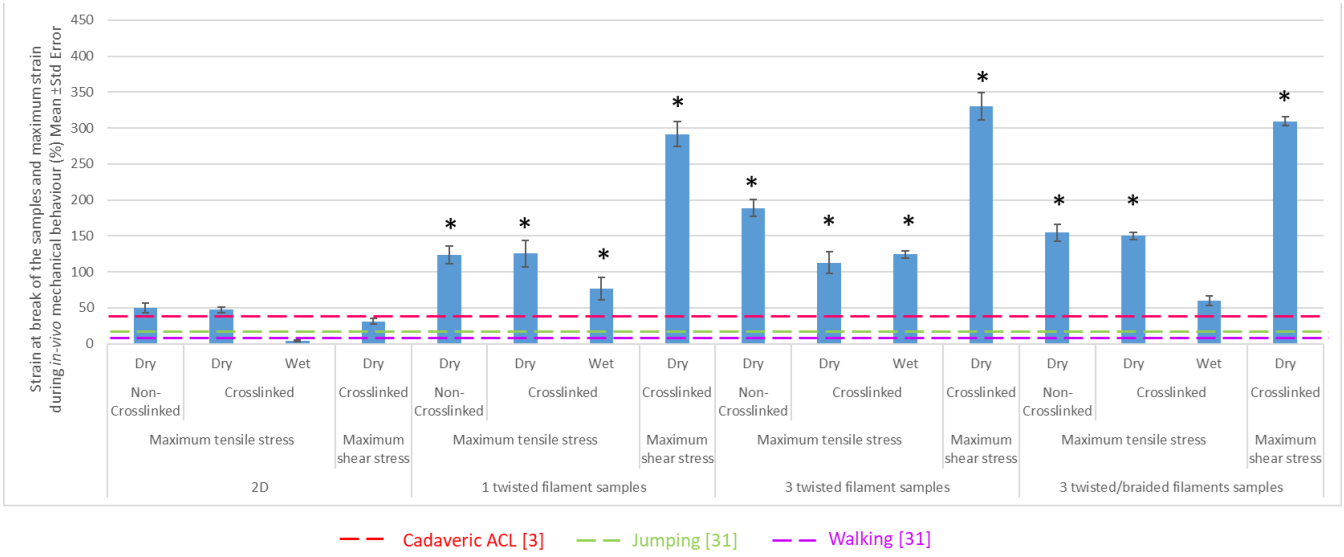

Figure 4. Strain at break (%) after 10 loading cycles per electrospun structure (Mean ± Std Dev). * Significant different with the cadaveric and *in-vivo* ACL (p value < 0.05).

It is also worth highlighting that more robust structures exhibited more consistent and reproducible mechanical properties than thinner structures, narrowing the standard deviation for structures such as 3 twisted filament scaffolds and 3 twisted/braided filament scaffolds.

MANOVA analysis showed that the structure, mechanical testing (tensile or simulate an anterior/posterior shear force), environmental condition (dry or wet samples) and structure/mechanical testing and structure/environmental condition interactions presented significant differences for the Young's modulus and ultimate tensile stress (P value < 0.0001). Also, significant differences were found in the values of ultimate tensile stress between crosslinked and non-crosslinked samples (P value < 0.0001). However, there were low significant differences in Young's modulus between crosslinked and non-crosslinked samples (P value = 0.036), and there were not significant differences in both Young's modulus and ultimate tensile stress for the interaction between crosslinked and structure (P value = 0.212 and P value = 0.226 respectively).

The importance of the independent variables on the dependent variables was analysed through the Eta values. In this analysis, it was observed that the structure and the interaction between structure and mechanical testing (tensile vs shear) highly influenced on the ultimate tensile stress with Eta values of 0.772 and 0.728 respectively, and the kind of structure and environmental condition (dry vs wet samples) highly affected to the Young's modulus with Eta values of 0.628 and 0.595.

The 10th cycle stress / strain curves were shown, for all the conditions and type of structures produced (one representative sample per structure were shown), in Figure 5. 2D corresponds to 2D scaffolds, 1TF to 1 twisted filament scaffolds, 3TB to 3 twisted filament scaffolds and 3TBF to 3 twisted/braided filament scaffolds.

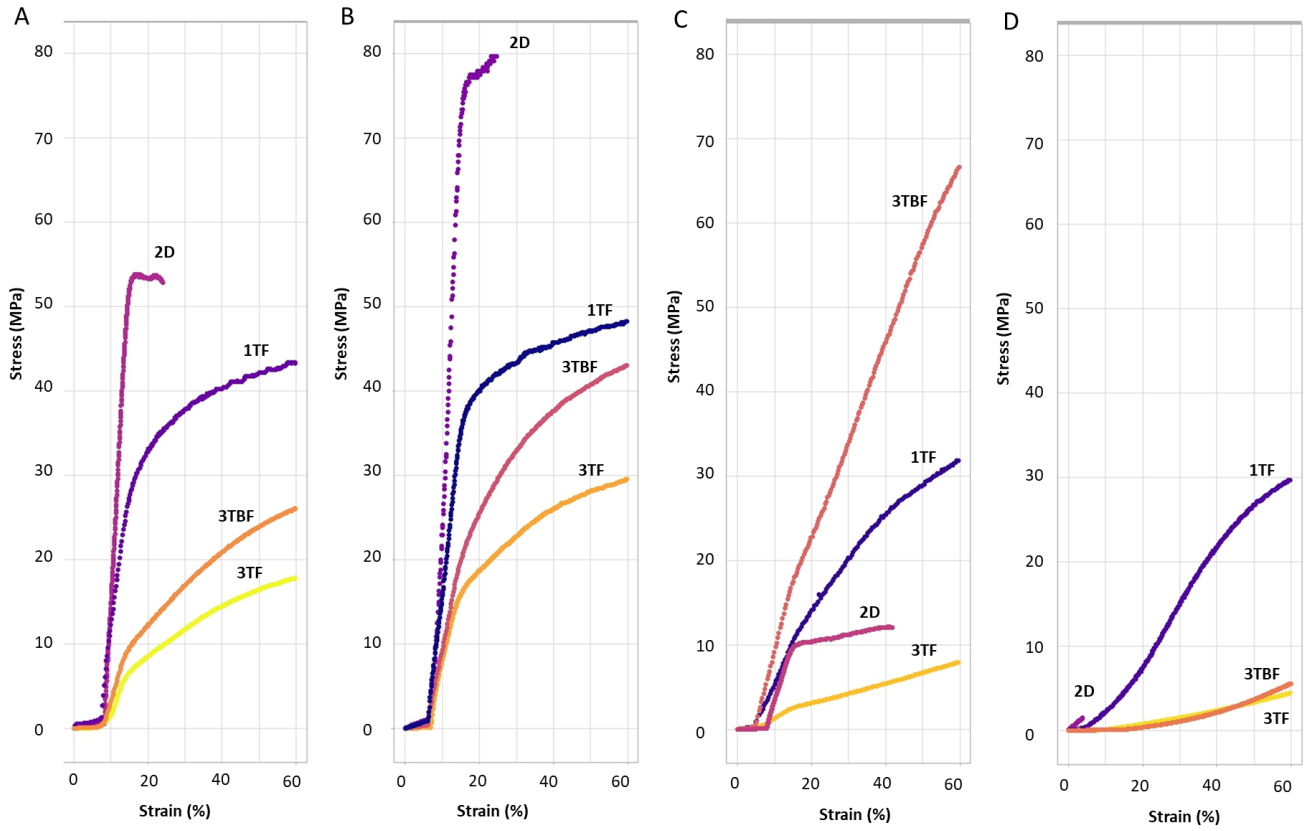

Figure 5. Stress (MPa) / Strain (%) per structure A) Non-crosslinked representative samples B) Crosslinked representative samples C) Representative samples under shear D) Wet crosslinked representative samples. All graphs were capped at 60% of strain.

Note that as all 3D scaffolds developed in this study exhibited higher strain at break than the one reported from cadaveric ACLs (44 ± 8% [3]) and higher than the maximum strain observed in our the *in-vivo* mechanical study (Figure 4), the stress-strain curve of our specimens was capped to 60% to clearly show the toe and linear regions, which were the most relevant regions to be compared to the *in-vivo* mechanical behaviour recorded from our participants while daily and high impact activities were performed.

Figure 5A and B shows that 2D and 1 twisted filament scaffolds experienced higher Young's modulus and ultimate tensile stress than 3 twisted filament scaffolds and 3 twisted/braided filament scaffolds. These figures also showed that less robust scaffolds, such as 2D and 1twisted filament scaffolds presented a plastic deformation in higher values of stress and strain than more robust scaffolds. Plastic deformation was experienced by non-crosslinked 2D and 1 twisted filament scaffolds from levels of stress above 54 MPa and 28-30 MPa respectively (Figure 5A); however, non-crosslinked 3 twisted filaments scaffolds and non-crosslinked 3 twisted/braided filaments deformed plastically in values below 10 MPa and strain values around 15% (Figure 5A).

Crosslinked samples presented a stiffer toe region, but a smoother inflection point than their non-crosslinked counterparts (Figure 5B). Moreover, all samples presented plastic deformation in values of stress higher than the non-crosslinked samples. 2D crosslinked scaffolds can reach levels of stress of 77-78 MPa before the plastic deformation, 1 twisted filament crosslinked scaffolds of around 38 MPa, 3 twisted filaments crosslinked scaffolds of around 18 MPa and 3 twisted/braided filaments crosslinked samples of 25 MPa.

Figure 5C showed the mechanical behaviour of the scaffolds tested simulating an anterior/posterior shear force. 2D scaffolds, 1 twisted filament scaffolds and 3 twisted filaments scaffolds presented plastic deformation from 16% strain; however, 3 twisted/braided filaments crosslinked samples faithfully recreated the ACL-like *in-vivo* response. Figure 6 shows the mean and standard deviation of experimental data from ten 3 twisted/braided filaments crosslinked samples and the *in-vivo* mechanical behaviour of the ACL calculated from the kinematics of our participants. As the *in-vivo* mechanical behaviour of the ACL did not reach values higher than 24.8 ± 2.2 MPa, data of our specimens were capped to 25 MPa, to clearly observed how faithfully the toe region and linear region were reproduced with our scaffolds.

A different mechanical behaviour was experienced in wet samples (Figure 5D). While 2D wet samples resulted in the most fragile with low levels of stress and strain, 1twisted filament scaffolds exhibited values of ultimate tensile stress of 37.2 ± 12.1 MPa comparable to the native ACL (38 MPa [3]) and strain at break higher than the natural ACL (Figure 4). All the wet samples smoothed the toe and the inflection point, experienced an elastic deformation until higher values of strain than the natural ACL (44 ± 8% [3]) and presented lower ultimate tensile stress and Young's modulus than their dry counterparts.

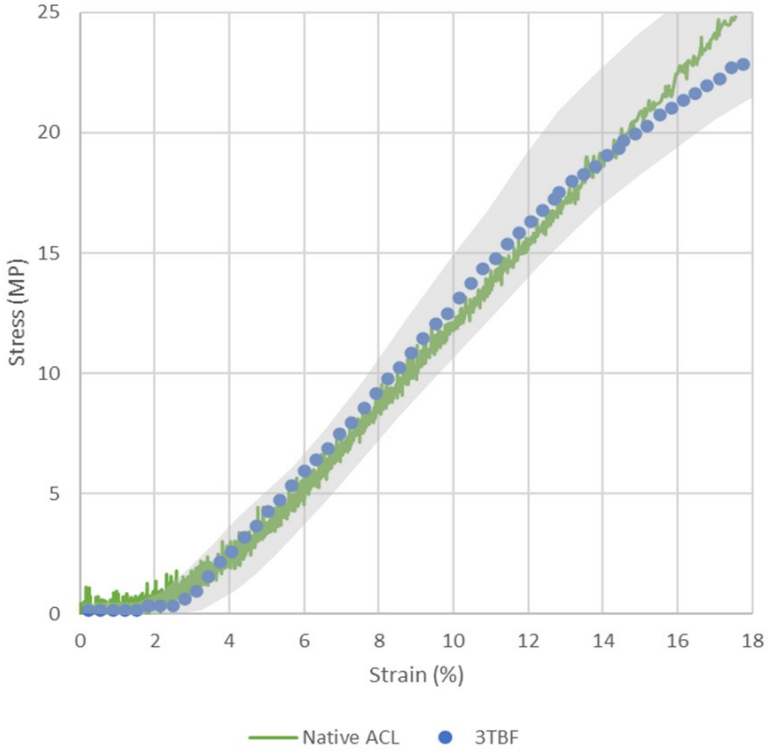

Figure 6. Stress (MPa) / Strain (%) for 3 twisted/braided filaments crosslinked structure versus *in-vivo* mechanical behaviour of the ACL. Graph was capped at 25MPa of stress.

PVA electrospun scaffolds showed comparable mechanical properties (Young's modulus and maximum tensile stress) to cadaveric studies of the ACL and presented an ACL-like *in-vivo* response. This fact is aligned to a previous study were PVA cords showed comparable mechanical properties as cadaveric ACL [16]. Our scaffolds exhibited better mechanical behaviour than other electrospun scaffolds manufactured with different materials for the same purpose [26,27,29,30].

3.1.2. Hyper-elastic and non-linear spring-based models

Biological soft tissues such as the ACL, present a non-linear stress/strain curve and can undergo reversible large strains and deformations under different loading conditions [50]. These characteristics cannot be simulated through linear elastic models; therefore, researchers have developed and used non-linear elastic models able to model large deformations and strains. Neo-Hookean, Mooney Rivlin, Ogden or Yeoh models are some of the most popular hyper-elastic strain energy density models used in soft tissues [50]. Mooney Rivlin model is used in this research to characterise both the hyper-elastic behaviour of our 3 twisted/braided filaments crosslinked samples and the *in-vivo* natural ACL.

Analysing the hyper-elastic behaviour of both structures, we observed that comparable models were produced with almost identical model coefficients (Figure 7). Model coefficients of 1.022 for C_1 and 0.977 for C_2 were obtained for the *in-vivo* ACL, whereas values of 1.019 for C_1 and 0.981 for C_2 were obtained for our scaffolds. These values were aligned to values previously reported by Peña *et al.* or Weiss *et al.* [5,49]. In addition, both models presented acceptable goodness of fit with coefficients of determination of 0.931 for the prediction of the hyper-elastic behaviour of the *in-vivo* natural ACL and 0.971 for the prediction of the hyper-elastic behaviour of our 3 twisted/braided filaments crosslinked scaffolds.

Some limitations associated with these models were that for both structures the material was considered as incompressible and time-dependant characteristics such as viscoelasticity, creep or relaxation were neglected. More realistic

approximations should include those characteristics. More experimental data and complex models will be considered in future research.

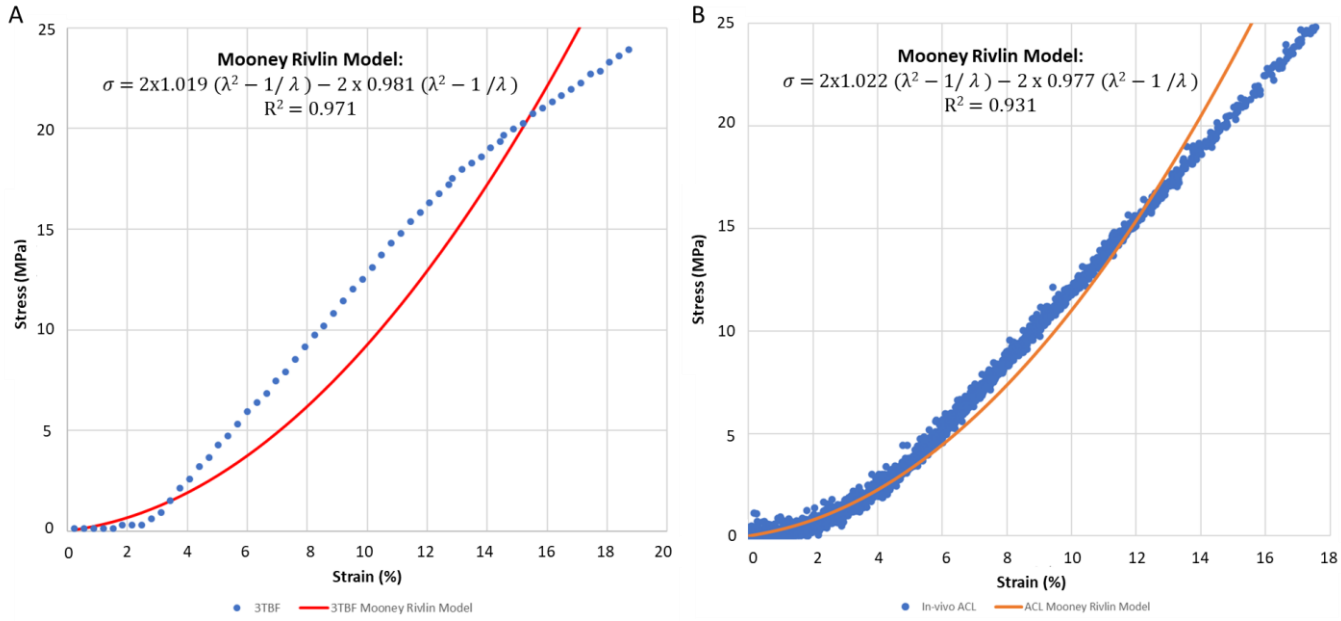

Figure 7. Stress (MPa) / Strain (%) for A) 3 twisted/braided filaments crosslinked structure and B) *in-vivo* mechanical behaviour of the ACL compared to Mooney Rivlin model. Graphs were capped at 25MPa of stress.

In addition to the hyper-elastic models presented above, novel high-accurate non-linear models were also evaluated for both *in-vivo* mechanical behaviour of the ACL and the scaffolds (Figure 8). The model proposed in this article is based on the Blankevoort and Huiskes model [41], where toe, linear and breaking regions were modelled. The parameter called A was used to define the toe region. Comparable values of these parameter were obtained for both structures, being 0.116 MPa for the scaffold and 0.143 MPa for the *in-vivo* ACL. Similarly, the values of the parameters k_1 and B were defined for the linear region and again comparable values were observed. K_1 of 1.720 MPa and B of 2.585 were obtained for the 3 twisted/braided filaments crosslinked scaffolds and k_1 of 1.711 MPa and B of 2.989 were obtained for the *in-vivo* natural ACL. To characterise the breaking region for our 3 twisted/braided filaments crosslinked scaffolds values of 3.915 for C and of 1.073 for k_2 were obtained.

The two main differences presented on these models were that no breaking region was observed in the *in-vivo* natural ACL, due to non-harmful activities were developed to collect the kinematic data of our participants and strains at transition point and inflection points were slightly different for both structures, being 4 the strain at transition point for our 3 twisted/braided filaments crosslinked scaffolds and 6 for the *in-vivo* ACL. The strain at the inflection point for the scaffolds were 13, whereas no inflection point was observed for the *in-vivo* native ACL.

Lastly, high coefficients of determination were obtained with these models, being these values 0.951 and 0.998 for the toe and linear region of the *in-vivo* ACL and 0.997, 0.999 and 0.999 for the toe, linear and breaking region of the scaffolds. These models presented a higher goodness of fit than the hyper-elastic models previously shown.

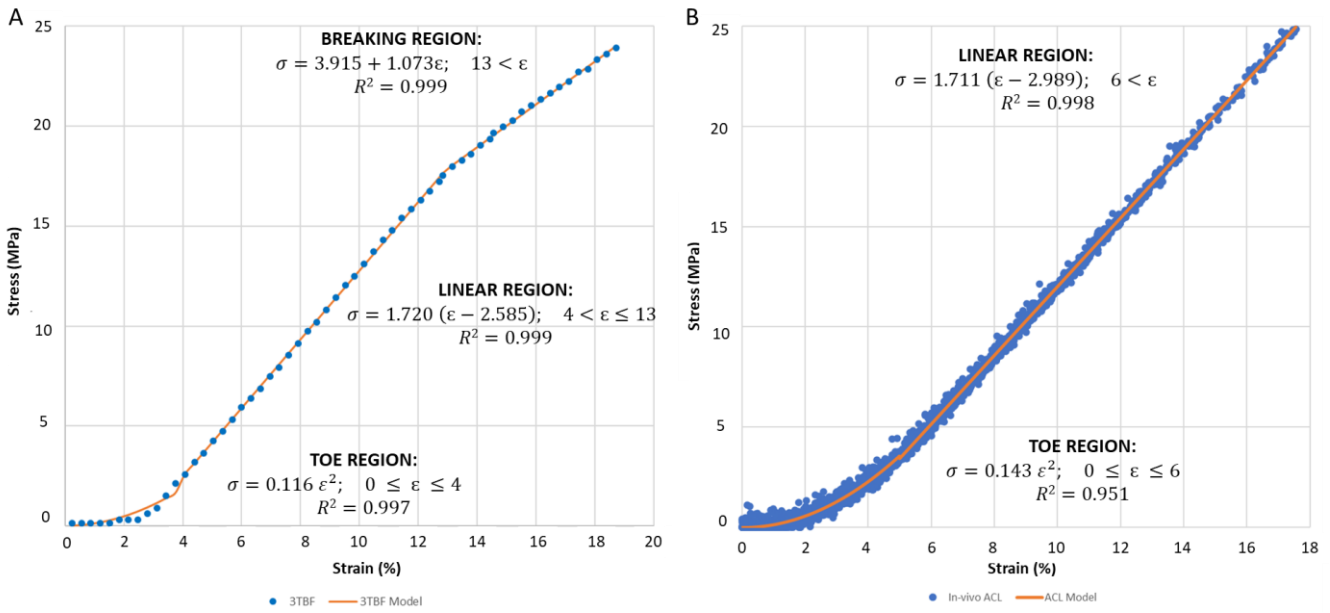

Figure 8. Stress (MPa) / Strain (%) for A) 3 twisted/braided filaments crosslinked structure and B) *in-vivo* mechanical behaviour of the ACL compared to a non-linear string-based model. Graphs were capped at 25MPa of stress.

3.2. Morphological characterisation

The production of 2D electrospun scaffolds generated a homogeneous network of fibres. The manufacturing of 3D structures allowed the creation of bundles of fibres and fascicles that were not present in the 2D structures, mimicking the morphology of the natural ACL.

The diameter of the PVA fibres in the 1 twisted filament non-crosslinked structure was 97 ± 5 nm, the thickness of the bundle of fibres was 8 ± 1µm and the size of the fascicles was 711 ± 19 µm. The diameter of PVA fibres for 3 twisted filaments non-crosslinked structure was 146 ± 8 nm, the thickness of the group of fibres was 25 ± 5 µm and the diameter of the fascicles was 614 ± 64 µm. In the case of the 3 twisted/braided filaments non-crosslinked structure, the mean diameter of the PVA fibres was 121 ± 6 nm, the thickness of the group of fibres was 18 ± 5 µm and the diameter of the fascicles was 593 ± 27 µm. Comparing these measurements with the diameters of the collagen fibrils, fibres and fascicules of the natural ACL (collagen fibrils: 40-150 nm, fibres: 1-20 µm, fascicles: 360-1500 µm [6–10]), all were in the same range of dimension as the structure of the collagen in the natural ligament and no significant differences were observed.

As it is appreciated in Figure 9, the nanofibres were not damaged in the manufacturing process and their diameter of the fibres were unmodified compared to the 2D electrospun scaffolds (P value > 0.05 between diameter of fibres for the 2D scaffolds and the 3D scaffolds developed in the present study).

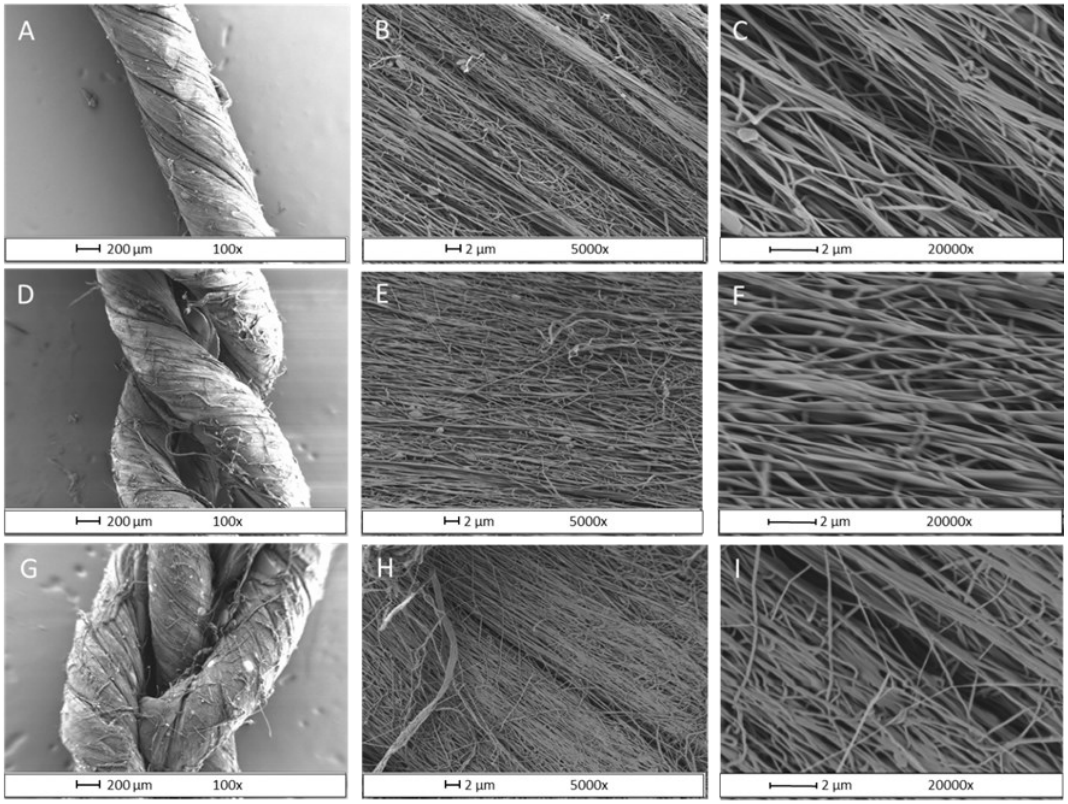

Figure 9. 1 twisted filament non-crosslinked samples A) 100x B) 5000x C) 20000x. 3 twisted filaments non-crosslinked samples D) 100x E) 5000x F) 20000x. 3 twisted/braided filaments non-crosslinked samples G) 100x H) 5000x I) 20000x

From the mechanical study, it was determined that the most suitable 3D structure to mimic the natural ACL properties, was the 3 twisted/braided filaments structure, therefore the morphological characterisation will be focussed on this type of structure for future research.

The same measurements were performed for 3 twisted/braided filaments crosslinked structure. The mean diameter of the crosslinked PVA fibres was 177 ± 19 nm, the thickness of the group of fibres was 18 ± 4 µm and the size of the fascicles was 675 ± 48 µm (Figure 10B). Comparing the crosslinked structure with the non-crosslinked (Figure 10A), it was observed that the diameter of the fibres significantly increased with the crosslinking (P value < 0.001).

When the crosslinked 3 twisted/braided filaments structures were immersed in PBS for 1 minute, the mean diameter resulted 461 ± 4 nm, the thickness of the group of fibres was 19 ± 3 µm and the size of the fascicles was 569 ± 9 µm (Figure 10C). Therefore, the morphology between dry and wet crosslinked 3 twisted/braided filaments structures resulted significantly different (P value < 0.0001). Although a swelling of the nanofibers was observed in wet conditions, previous studies with PVA electrospun scaffolds reported excellent cell adhesion and proliferation with values of fibre diameter between 379 ± 37 nm and 524 ± 31 nm [51].

In the case of the 3 twisted/braided filaments structures already tensile tested, the mean diameter of the PVA fibres was 110 ± 9 nm, the thickness of the group of fibres was 28 ± 8 µm and the diameter of the fascicles was 496 ± 22 µm. Moreover, it was observed that this structure post tensile testing (Figure 10D) had fibres with no preferential orientation comparable to damaged ACL reported by Provenzano *et al.* [52].

In this last study it was observed that the diameter of the fibres and the diameter of the fascicules were reduced in the tested samples. This was due to the fascicles and fibres being stretched during the tensile tests, reducing their diameters. However, the thickness of the group of fibres increased after being tested, this was because the groups of fibres after the test were closer to one each other, increasing the thickness of the group of fibres.

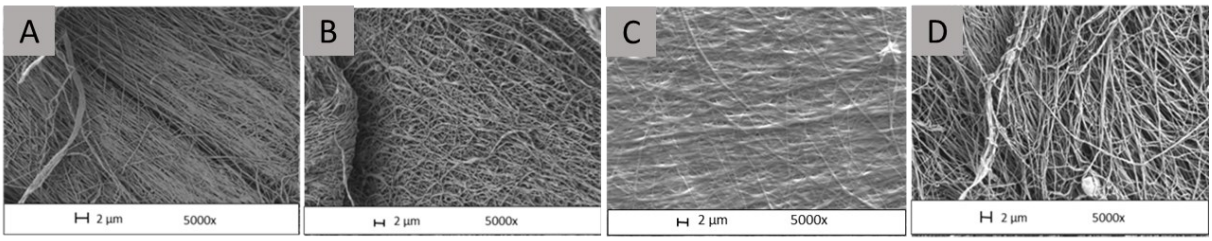

Figure 10. 3 twisted/braided filaments samples A) non-crosslinked sample B) crosslinked sample C) crosslinked sample in wet condition D) non-crosslinked sample after tensile testing

In addition, the diameter distribution of the non-crosslinked 3 twisted/braided filaments samples was evaluated and compared to the diameter distribution of the fibrils of collagen in healthy rabbit's ACLs following a recent study [12]. In that study, Kadyr *et al*. reported diameters of the collagen fibril of 113.5±2.4 nm and weighted average diameter of 124.3±2.4 nm, non-significantly different to the diameter of the PVA fibres obtained with our non-crosslinked 3 twisted/braided filaments samples (121 ± 6 nm). A bimodal distribution of the diameters was observed in healthy rabbit's ACLs, where two peaks were observed in diameters of 95±10 nm and in diameters of 160 nm [12], whereas in our study a bimodal distribution was observed in diameters of 90 nm and 130 nm (Figure 11). These findings are in agreement to the distribution of the diameters observed in healthy ACLs.

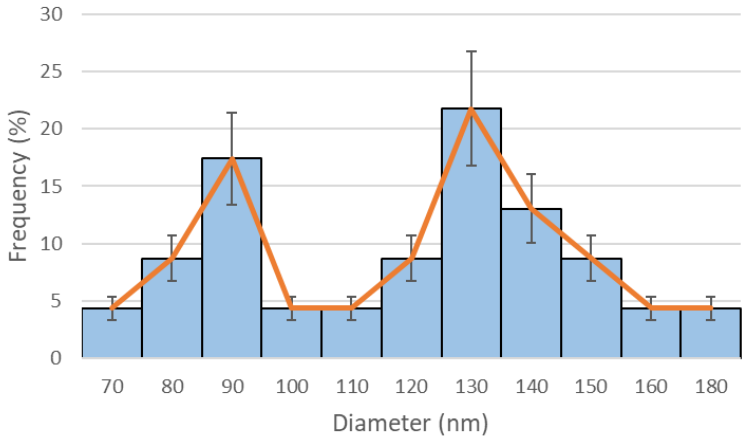

Figure 11. Histogram and polygon of frequencies of non-crosslinked 3 twisted/braided filaments samples. Error bars represent standard deviation (n=10).

4. Conclusions

This study evaluated and compared for the first time 2D and multiple 3D electrospun structures with the goal of determining which structure reproduces more faithfully the *in-vivo* mechanical behaviour of the natural ACL. Besides their hyper-elastic character of both *in-vivo* ACL and the manufactured scaffolds was assessed for the first time to produce biomimetic electrospun scaffolds, being this approach extrapolated to other tissue replacements.

The mechanical behaviour of the 3 twisted/braided filaments crosslinked structure demonstrated non-significant differences with the native ACL following our initial assessment where only the elastic properties of the structures were assessed. This structure produced a maximum tensile stress of 38 ± 3 MPa and a Young's modulus of 129 MPa comparable to the 38 MPa and 111 MPa respectively reported for the natural ACL [3] in dry conditions. Analysing the hyper-elastic *in-vivo* mechanical behaviour of the ACL and the hyper-elastic behaviour of 3 twisted/braided filaments crosslinked structure was observed that both followed comparable experimental curves and Mooney Rivlin curves with almost identical coefficients (being C_1 1.022 and C_2 0.977 for the *in-vivo* ACL and C_1 1.019 and C_2 0.981 for the scaffold) and coefficients of determination of 0.931 and 0.971 respectively. Novel high-accurate non-linear models evaluated for both *in-vivo* mechanical behaviour of the ACL and the scaffolds also presented comparable coefficients and coefficients of determination of 0.951 and 0.998 for the toe and linear region of the *in-vivo* ACL and 0.997, 0.999 and 0.999 for the

toe, linear and breaking region of the scaffolds. Demonstrating that the manufactured scaffolds exhibited an ACL-like mechanical response.

In terms of morphology, biomimetic 3D electrospun scaffolds were created. The dimension of the PVA fibres, bundle of fibres and fascicles agreed with the diameters of the collagen fibrils, fibres and fascicles in the natural ligament. The distribution of the diameter of the fibres follows a bimodal pattern comparable to the one reported in healthy ACLs. It was also demonstrated that the manufacturing process did not damage the nanofibres and their nano-morphology was not modified. Moreover, this process mimicked the hierarchical structure of the native ACL and created bundles of fibres easily measurable with a SEM. In addition, after a tensile test to failure, the morphology of the 3D structure was visually comparable to the morphology of the collagen fibres of a damaged ACL reported in a previous study [52].

In conclusion, within the current confines of this study, it was demonstrated that the 3 twisted/braided filaments scaffolds are the most suitable structure to be used as a replacement for the ACL. Further work will be done to assess the cell behaviour on our scaffolds and investigate crosslinking alternatives to the glutaraldehyde, such as polydopamine, saccharides or physical crosslinking, to eliminate the toxicity of the scaffolds and tailor the degradation rate.

Author Contributions: Conceptualization, E.R.; methodology, E.R., K.A, G.C, N.R.; formal analysis, E.R.; investigation, E.R.; writing—original draft preparation, E.R.; writing—review and editing, E.R., K.A, G.C, N.R.; supervision, K.A, G.C, N.R. All authors have read and agreed to the published version of the manuscript.

Data Availability Statement: The data supporting this article will be made available on request to the correspondence author Elisa.Roldan-Ciudad@mmu.ac.uk.

Acknowledgments: Some experimental work included in this study was partially performed in the Manchester Institute of Biotechnology (University of Manchester). The authors would like to acknowledge Professor Paulo Jorge Da Silva Bartolo for his support allowing the use of the University of Manchester facilities. The authors would also like to thank the technical staff of the Manchester Metropolitan University, Mike Green, Hayley Andrews and Greg May for training ER on the use of the tensiometer, SEM, Vicon System and MRI.

Conflicts of Interest: The authors declare no conflict of interest.

References

[1] C.T. Laurencin, J.W. Freeman, Ligament tissue engineering: an evolutionary materials science approach, Biomaterials 26 (2005) 7530–7536. https://doi.org/10.1016/j.biomaterials.2005.05.073.

[2] N.L. Leong, F.A. Petrigliano, D.R. McAllister, Current tissue engineering strategies in anterior cruciate ligament reconstruction, J Biomed Mater Res A 102 (2014) 1614–1624. https://doi.org/10.1002/jbm.a.34820.

[3] F.R. Noyes, E.S. Grood, The strength of the anterior cruciate ligament in humans and Rhesus monkeys, J Bone Jt. Surg Am 58 (1976) 1074–1082.

[4] J.C. Gardiner, J.A. Weiss, Subject-specific finite element analysis of the human medial collateral ligament during valgus knee loading, J. Orthop. Res. 21 (2003) 1098–1106. https://doi.org/10.1016/S0736-0266(03)00113-X.

[5] E. Peña, B. Calvo, M.A. Martínez, M. Doblaré, A three-dimensional finite element analysis of the combined behavior of ligaments and menisci in the healthy human knee joint, J. Biomech. 39 (2006) 1686–1701. https://doi.org/10.1016/j.jbiomech.2005.04.030.

[6] K. Shino, B.W. Oakes, S. Horibe, K. Nakata, N. Nakamura, Collagen fibril populations in human anterior cruciate ligament allografts. Electron microscopic analysis, Am. J. Sports Med. 23 (1995) 203–208; discussion 209. https://doi.org/10.1177/036354659502300213.

[7] H.D. Moeller, U. Bosch, B. Decker, Collagen fibril diameter distribution in patellar tendon autografts after posterior cruciate ligament reconstruction in sheep: changes over time., J. Anat. 187 (1995) 161–167.

[8] S. Bancelin, C. Aimé, I. Gusachenko, L. Kowalczuk, G. Latour, T. Coradin, M.-C. Schanne-Klein, Determination of collagen fibril size via absolute measurements of second-harmonic generation signals, Nat. Commun. 5 (2014). https://doi.org/10.1038/ncomms5920.

[9] R. Strocchi, V. De Pasquale, A. Facchini, M. Raspanti, S. Zaffagnini, M. Marcacci, Age-related changes in human anterior cruciate ligament (ACL) collagen fibrils, Ital. J. Anat. Embryol. Arch. Ital. Anat. Ed Embriologia 101 (1996) 213–220.

[10] E. Roldán, N.D. Reeves, G. Cooper, K. Andrews, Towards the ideal vascular implant: Use of machine learning and statistical approaches to optimise manufacturing parameters, Front. Phys. 11 (2023). https://doi.org/10.3389/fphy.2023.1112218.

[11] S. Smatov, F. Mukasheva, C. Erisken, Collagen Fibril Diameter Distribution of Sheep Anterior Cruciate Ligament, Polymers 15 (2023) 752. https://doi.org/10.3390/polym15030752.

[12] S. Kadyr, U. Nurmanova, B. Khumyrzakh, A. Zhakypbekova, D. Saginova, N. Daniyeva, C. Erisken, Braided biomimetic PCL grafts for anterior cruciate ligament repair and regeneration, Biomed. Mater. Bristol Engl. 19 (2024). https://doi.org/10.1088/1748-605X/ad2555.

[13] P. Supaphol, S. Chuangchote, On the electrospinning of poly(vinyl alcohol) nanofiber mats: A revisit, J. Appl. Polym. Sci. 108 (2008) 969–978. https://doi.org/10.1002/app.27664.

[14] J.-C. Park, T. Ito, K.-O. Kim, K.-W. Kim, B.-S. Kim, M.-S. Khil, H.-Y. Kim, I.-S. Kim, Electrospun poly(vinyl alcohol) nanofibers: effects of degree of hydrolysis and enhanced water stability, Polym. J. 42 (2010) 273–276. https://doi.org/10.1038/pj.2009.340.

[15] N. Jain, V.K. Singh, S. Chauhan, A review on mechanical and water absorption properties of polyvinyl alcohol based composites/films, J. Mech. Behav. Mater. 26 (2017) 213–222. https://doi.org/10.1515/jmbm-2017-0027.

[16] J.S. Bach, F. Detrez, M. Cherkaoui, S. Cantournet, D.N. Ku, L. Corté, Hydrogel fibers for ACL prosthesis: Design and mechanical evaluation of PVA and PVA/UHMWPE fiber constructs, J. Biomech. 46 (2013) 1463–1470. https://doi.org/10.1016/j.jbiomech.2013.02.020.

[17] J.W. Freeman, M.D. Woods, C.T. Laurencin, Tissue engineering of the anterior cruciate ligament using a braid-twist scaffold design, J. Biomech. 40 (2007) 2029–2036. https://doi.org/10.1016/j.jbiomech.2006.09.025.

[18] Hudson PB, Clapp AC, Kness D. Joseph's, Introductory Textile Science., 6. Harcourt Brace Jovanovich College Publishers; New York, 1993.

[19] Cooper JA., Design, Optimization and In Vivo Evaluation of a Tissue-Engineered Anterior Cruciate Ligament Replacement., Drexel University Press; Philadelphia, 2002.

[20] G.H. Altman, R.L. Horan, H.H. Lu, J. Moreau, I. Martin, J.C. Richmond, D.L. Kaplan, Silk matrix for tissue engineered anterior cruciate ligaments, Biomaterials 23 (2002) 4131–4141.

[21] J. Chen, G.H. Altman, V. Karageorgiou, R. Horan, A. Collette, V. Volloch, T. Colabro, D.L. Kaplan, Human bone marrow stromal cell and ligament fibroblast responses on RGD-modified silk fibers, J. Biomed. Mater. Res. A 67 (2003) 559–570. https://doi.org/10.1002/jbm.a.10120.

[22] H.H. Lu, J.A. Cooper, S. Manuel, J.W. Freeman, M.A. Attawia, F.K. Ko, C.T. Laurencin, Anterior cruciate ligament regeneration using braided biodegradable scaffolds: in vitro optimization studies, Biomaterials 26 (2005) 4805–4816. https://doi.org/10.1016/j.biomaterials.2004.11.050.

[23] J.A. Cooper, H.H. Lu, F.K. Ko, J.W. Freeman, C.T. Laurencin, Fiber-based tissue-engineered scaffold for ligament replacement: design considerations and in vitro evaluation, Biomaterials 26 (2005) 1523–1532. https://doi.org/10.1016/j.biomaterials.2004.05.014.

[24] G. Vunjak-Novakovic, G. Altman, R. Horan, D.L. Kaplan, Tissue engineering of ligaments, Annu. Rev. Biomed. Eng. 6 (2004) 131–156. https://doi.org/10.1146/annurev.bioeng.6.040803.140037.

[25] E. Roldan, N. Reeves, G. Cooper, K. Andrews, Optimization of manufacturing parameters through machine learning techniques to create biomimetic vascular implants, TISSUE Eng. PART A 29 (2023). https://doi.org/10.1089/ten.tea.2023.29043.abstracts.

[26] L.A. Bosworth, N. Alam, J.K. Wong, S. Downes, Investigation of 2D and 3D electrospun scaffolds intended for tendon repair, J. Mater. Sci. Mater. Med. 24 (2013) 1605–1614. https://doi.org/10.1007/s10856-013-4911-8.

[27] A. Sensini, C. Gualandi, L. Cristofolini, G. Tozzi, M. Dicarlo, Gabriella Teti, M. Mattioli-Belmonte, M.L. Focarete, Biofabrication of bundles of poly(lactic acid)-collagen blends mimicking the fascicles of the human Achille tendon, Biofabrication 9 (2017). https://doi.org/10.1088/1758-5090/aa6204.

[28] C. Erisken, X. Zhang, K.L. Moffat, W.N. Levine, H.H. Lu, Scaffold Fiber Diameter Regulates Human Tendon Fibroblast Growth and Differentiation, Tissue Eng. Part A 19 (2013) 519–528. https://doi.org/10.1089/ten.tea.2012.0072.

[29] P.-A. Mouthuy, N. Zargar, O. Hakimi, E. Lostis, A. Carr, Fabrication of continuous electrospun filaments with potential for use as medical fibres, Biofabrication 7 (2015). https://doi.org/10.1088/1758-5090/7/2/025006.

[30] B.B. Rothrauff, B.B. Lauro, G. Yang, R.E. Debski, V. Musahl, R.S. Tuan, Braided and Stacked Electrospun Nanofibrous Scaffolds for Tendon and Ligament Tissue Engineering, Tissue Eng. Part A 23 (2017) 378–389. https://doi.org/10.1089/ten.TEA.2016.0319.

[31] E. Roldán, N.D. Reeves, G. Cooper, K. Andrews, In vivo mechanical behaviour of the anterior cruciate ligament: A study of six daily and high impact activities, Gait Posture 58 (2017) 201–207. https://doi.org/10.1016/j.gaitpost.2017.07.123.

[32] E. Roldán, N.D. Reeves, G. Cooper, K. Andrews, Can we achieve biomimetic electrospun scaffolds with gelatin alone?, Front. Bioeng. Biotechnol. 11 (2023). https://doi.org/10.3389/fbioe.2023.1160760.

[33] K.A. Taylor, H.C. Cutcliffe, R.M. Queen, G.M. Utturkar, C.E. Spritzer, W.E. Garrett, L.E. DeFrate, In vivo measurement of ACL length and relative strain during walking, J Biomech 46 (2013) 478–483. https://doi.org/10.1016/j.jbiomech.2012.10.031 10.1016/j.jbiomech.2012.10.031. Epub 2012 Nov 21.</p>.

[34] K.A. Jisa, B.T. Williams, J.R. Jaglowski, T.L. Turnbull, R.F. LaPrade, C.A. Wijdicks, Lack of consensus regarding pretensioning and preconditioning protocols for soft tissue graft reconstruction of the anterior cruciate ligament, Knee Surg. Sports Traumatol. Arthrosc. 24 (2016) 2884–2891. https://doi.org/10.1007/s00167-015-3530-y.

[35] E. Roldán, Design and development of new ligament implants, doctoral, Manchester Metropolitan University, 2018. https://e-space.mmu.ac.uk/622840/ (accessed June 5, 2023).

[36] E. Roldan, N. Reeves, G. Cooper, K. Andrews, Physiological mechanical testing and in-vivo mechanical behaviour to inform the production of biomimetic tissue engineered ligaments, TISSUE Eng. PART A 29 (2023). https://doi.org/10.1089/ten.tea.2023.29043.abstracts.

[37] G.G. Arliani, D.C. Astur, E.R. Moraes, C.C. Kaleka, W. Jalikjian, P. Golano, M. Cohen, Three dimensional anatomy of the anterior cruciate ligament: a new approach in anatomical orthopedic studies and a literature review, Open Access J. Sports Med. 3 (2012) 183–188. https://doi.org/10.2147/OAJSM.S37203.

[38] X. Dai, Y. Cai, Measurement of anterior cruciate ligament angles in single-bundle reconstruction using the anteromedial portal, Am. J. Orthop. Belle Mead NJ 41 (2012) 268–272.

[39] Y. Cho, J. Cho, D. Kim, Normal sagittal of the anterior cruciate ligament can be reproduced using accessory anteromedial portal technique: a magnetic resonance imaging study, Arch. Orthop. Trauma Surg. 132 (2012) 1011–1019. https://doi.org/10.1007/s00402-012-1498-3.

[40] J.C. Reid, B. Yonke, M. Tompkins, The angle of inclination of the native ACL in the coronal and sagittal planes, Knee Surg. Sports Traumatol. Arthrosc. Off. J. ESSKA 25 (2017) 1101–1105. https://doi.org/10.1007/s00167-017-4419-8.

[41] L. Blankevoort, R. Huiskes, Ligament-bone interaction in a three-dimensional model of the knee, J Biomech Eng 113 (1991) 263–269.

[42] S.D. Łagan, A. Liber-Kneć, Experimental testing and constitutive modeling of the mechanical properties of the swine skin tissue, Acta Bioeng. Biomech. 19 (2017) 93–102. https://doi.org/10.5277/ABB-00755-2016-02.

[43] E. Roldán, N.D. Reeves, G. Cooper, K. Andrews, Design Consideration for ACL Implants based on Mechanical Loading, Procedia CIRP 49 (2016) 133–138. https://doi.org/10.1016/j.procir.2015.11.002.

[44] J.C. Reid, B. Yonke, M. Tompkins, The angle of inclination of the native ACL in the coronal and sagittal planes, Knee Surg. Sports Traumatol. Arthrosc. Off. J. ESSKA 25 (2017) 1101–1105. https://doi.org/10.1007/s00167-017-4419-8.

[45] N. Pujol, S. Queinnec, P. Boisrenoult, A. Maqdes, P. Beaufils, Anatomy of the anterior cruciate ligament related to hamstring tendon grafts. A cadaveric study, Knee 20 (2013) 511–514. https://doi.org/10.1016/j.knee.2012.10.006.

[46] FAQ/effectSize - CBU statistics Wiki, (2022). https://imaging.mrc-cbu.cam.ac.uk/statswiki/FAQ/effectSize (accessed October 24, 2022).

[47] S. Kawabata, M. Niwa, Fabric Performance in Clothing and Clothing Manufacture, J. Text. Inst. 80 (1989) 19–50. https://doi.org/10.1080/00405008908659184.

[48] V.I. Walters, Design and Analysis of a Collagenous Anterior Cruciate Ligament Replacement, Thesis, Virginia Tech, 2011. https://vtechworks.lib.vt.edu/handle/10919/32458 (accessed March 24, 2018).

[49] J.A. Weiss, J.C. Gardiner, C. Bonifasi-Lista, Ligament material behavior is nonlinear, viscoelastic and rate-independent under shear loading, J. Biomech. 35 (2002) 943–950. https://doi.org/10.1016/S0021-9290(02)00041-6.

[50] H.B. Khaniki, M.H. Ghayesh, R. Chin, M. Amabili, Hyperelastic structures: A review on the mechanics and biomechanics, Int. J. Non-Linear Mech. 148 (2023) 104275. https://doi.org/10.1016/j.ijnonlinmec.2022.104275.

[51] S. Chahal, F.S.J. Hussain, A. Kumar, M.S.B.A. Rasad, M.M. Yusoff, Fabrication, characterization and in vitro biocompatibility of electrospun hydroxyethyl cellulose/poly (vinyl) alcohol nanofibrous composite biomaterial for bone tissue engineering, Chem. Eng. Sci. 144 (2016) 17–29. https://doi.org/10.1016/j.ces.2015.12.030.

[52] P.P. Provenzano, D.A. Martinez, R.E. Grindeland, K.W. Dwyer, J. Turner, A.C. Vailas, R. Vanderby, Hindlimb unloading alters ligament healing, J. Appl. Physiol. Bethesda Md 1985 94 (2003) 314–324. https://doi.org/10.1152/japplphysiol.00340.2002.